

pubs.acs.org/NanoLett Letter

Ferroelastic Nanodomain-mediated Mechanical Switching of Ferroelectricity in Thick Epitaxial Films

Qian Li,*,# Bo Wang,# Qian He, Pu Yu, Long-Qing Chen, Sergei V. Kalinin,* and Jing-Feng Li*



Cite This: Nano Lett. 2021, 21, 445-452



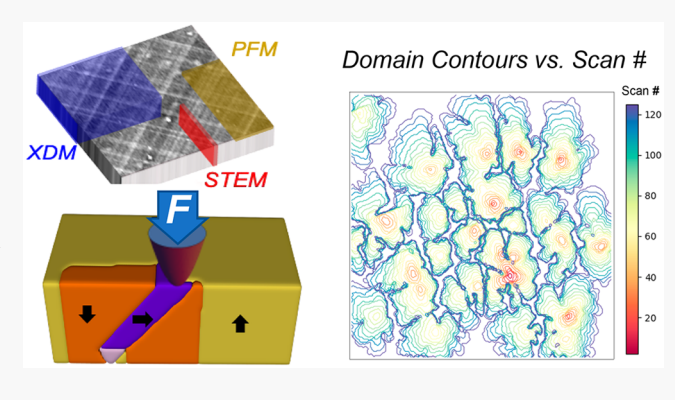
ACCESS

Metrics & More

Article Recommendations

Supporting Information

ABSTRACT: Mechanical switching of ferroelectric polarization, typically realized via a scanning probe, holds promise in (multi)ferroic device applications. Whereas strain gradient-associated flexoelectricity has been regarded to be accountable for mechanical switching in ultrathin (<10 nm) films, such mechanism can hardly be extended to thicker materials due to intrinsic short operating lengths of flexoelectricity. Here, we demonstrate robust mechanical switching in ~100 nm thick $Pb(Zr_{0.2}Ti_{0.8})O_3$ epitaxial films with a characteristic microstructure consisting of nanosized ferroelastic domains. Through a combination of multiscale structural characterizations, piezoresponse force microscopy, and phase-field simulations, we reveal that the ferroelastic nanodomains effectively mediate the 180° switching



nucleation in a dynamical manner during tip scanning. Coupled with microstructure engineering, this newly revealed mechanism could boost the utility of mechanical switching through extended material systems. Our results also provide insight into competing polarization switching pathways in complex ferroelectric materials, essential for understanding their electromechanical response.

KEYWORDS: ferroelectric thin films, polarization switching, mechanical switching, piezoreponse force microscopy, phase-field simulation

■ INTRODUCTION

The switching of one or multiple order parameters under external fields is the hallmark behavior of ferroics, and understanding the microscopic mechanisms of various switching processes comprises a crucial task in ferroic studies. For ferroelectrics, polarization switching is directly tied to the operation of many of their functional devices such as nonvolatile memories, memristors, domain wall electronics, and multiferroic heterojunctions.²⁻⁶ Ferroelectric switching is naturally realized by application of an electric field that aligns the polarization vector along the field direction due to electrostatic coupling. By contrast, uniaxial mechanical pressure primarily drives non-180° ferroelastic domain switching in multiaxial ferroelectrics while, in principle, not causing a 180° reversal of the polarization since both domain states are elastically equivalent. 7,8 There have been, however, intriguing mechanical switching phenomena (here we specifically refer to the 180° polarization reversal) locally driven via a piezoresponse force microscopy (PFM) tip, first reported in $BaTiO_3$ ultrathin (5 nm) films and later in ferroelectric (-like) $SrTiO_3$ and $LaAlO_3$ thin films. $^{10-13}$ These results indicate a new, nonelectrical means of polarization control that could find versatile device applications. In explaining such switching phenomena, Lu et al. proposed a mechanism invoking flexoelectricity; that is, the applied tip force induces a large strain gradient nearby at the film surface which generates a high internal electric field opposite to the pristine polarization vector.

The observation of mechanical switching, in turn, has been broadly regarded as an experimental illustration of flexoelectricity. ^{14,15}

Although flexoelectricity stands a plausible mechanism, tip pressure can initiate other concomitant bulk and surface processes, including ferroelastic switching, 16 polarization rotation, ^{17,18} and redistribution of surface adsorbate charge ¹⁹ and mobile lattice defects.²⁰ Besides this, the local pressure distribution during tip scanning can be more complex and dynamical than a static indentation scenario. 21 All these factors are intimately coupled within the thermodynamics of ferroelectric materials and may potentially lead to competing switching pathways, as predicted by recent theoretical studies. ²²⁻²⁵ Cao et al. showed that the contribution of tip-Cao et al. showed that the contribution of tipinduced flexoelectricity in Pb(Zr_{0.2}Ti_{0.8})O₃ substantially decreases when the film thickness is above ~25 nm. 22 The existence of such a thickness limit appears to be in line with previous studies that were predominantly based on ultrathin films, posing a severe constraint for practical applications since

Received: September 25, 2020 Revised: November 25, 2020 Published: December 2, 2020





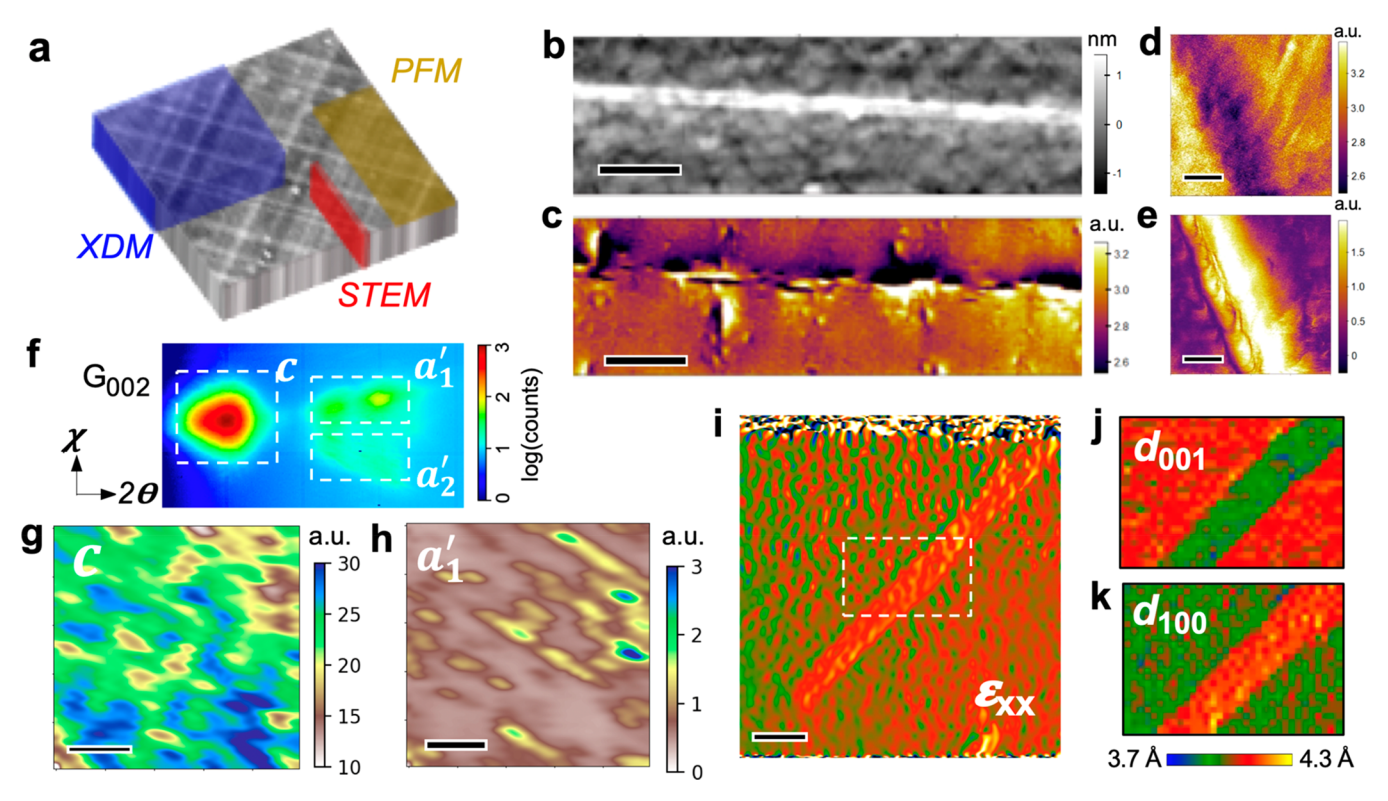


Figure 1. Multiscale characterizations of 100 nm Pb($Zr_{0.2}Ti_{0.8}$)O₃ thin films. (a) Schematic of the characterization modalities overlaid with PFM surface morphology; (b) morphology and (c) vertical piezoresponse amplitude maps over a ridge region (scale bar = 1 μ m); and (d) vertical and (e) lateral piezoresponse amplitude maps over a zoomed-in ridge region (scale bar = 50 nm). X-ray diffraction microscopy: (f) portion of the two-dimensional detector image summed from all scan locations, showing ROIs defined for the diffraction intensities of the c-domain and a_1'/a_2' -nanodomains, and (g, h) diffraction contrast maps corresponding to the two ROIs for the c- and a_1' -domains, respectively (scale bar = 5 μ m). STEM: (i) Geometrical phase analysis (GPA)-derived in-plane strain map of a near-surface region containing a single a'-nanodomain (scale bar = 5 nm) and the (j) out-of-plane and (k) in-plane lattice spacing maps derived from the Pb sublattice for a region enclosed in (i).

the fabrication and device integration of high-quality ultrathin films are technically demanding. Likewise, another study established the competing roles of depolarization field, shear strain, and flexoelectricity over a large parametric space for $\rm BaTiO_3$ thin films. 23 It is thus evident that mechanical switching in thin-film ferroelectrics could involve a rich variety of material-dependent microscopic mechanisms awaiting further exploration.

Here, we demonstrate robust mechanical switching in tetragonal-phase Pb(Zr_{0.2}Ti_{0.8})O₃ (PZT) epitaxial films with a thickness of ~100 nm, significantly larger than the previously studied materials. Through a combination of multiscale structural and piezoresponse characterizations with highveracity phase-field modeling, we have identified a heretofore unknown mechanism that the 180° polarization reversal can be dynamically mediated by nanosized ferroelastic a-domains native to the partially relaxed films as a defect type. Also, an intriguing continuous mechanical switching process has been captured, revealing rich details about the local switching dynamics. Our results not only advance the understanding of mechanical switching that could accelerate the exploitations of such a functionality in (multi)ferroic devices but also shed fresh light on complex electromechanical phenomena in ferroelectric materials.

■ RESULTS

In this study, we focus on thick (\sim 100 nm) PZT films epitaxially grown on SrTiO₃(001) substrates with SrRuO₃ as bottom electrodes. Due to the film thickness exceeding a critical value, ²⁶

the pristine films are partially relaxed and deviate from a fully strained, pure tetragonal c-domain structure, as has been thoroughly characterized over multiple length scales (see Figure 1a). The surface morphology of the films show cross-hatch line ridges that protrude by \sim 1 nm in height and run along both the in-plane [100]/[010] directions with varying separations of $\sim 0.5-1 \ \mu \text{m}$. Across these ridges, the measured (vertical) piezoresponse amplitude exhibits a systematic modulation with up to ~30% suppression/enhancement for the two opposite sides (Figure 1c); nevertheless, the corresponding piezoresponse phase (not shown) retains a constant sign as determined by an upward polarized c-domain matrix of the films. Lateral PFM measurement shows nonvanished piezoresponse over narrow regions around the ridges (typically <50 nm; cf. Figure 1d and e) while the signals are dominated by noise elsewhere, indicating a net in-plane polarization component in the former regions. The occurrence of such in-plane polarized inclusions, referred as a'(minor)-domains here, is confirmed through nanofocused X-ray diffraction microscopy (XDM).²⁷ Figure 1f presents a typical 002 diffraction pattern of the PZT films, acquired at a rocking angle with a maximum intensity of a'domains. Compared with the diffraction peak of the c-domain matrix, those of the a'-domains appear at higher 2θ angles and are offset by up to $\pm 0.5^{\circ}$ in the χ angle (transverse to the incident X-rays), consistent with their smaller out-of-plane lattice parameters and associated lattice tilts. The scattering intensities of the a'-domains are weak and much diffused, further suggesting their minor population in the films. The real-space distribution maps of these domains are obtained from the

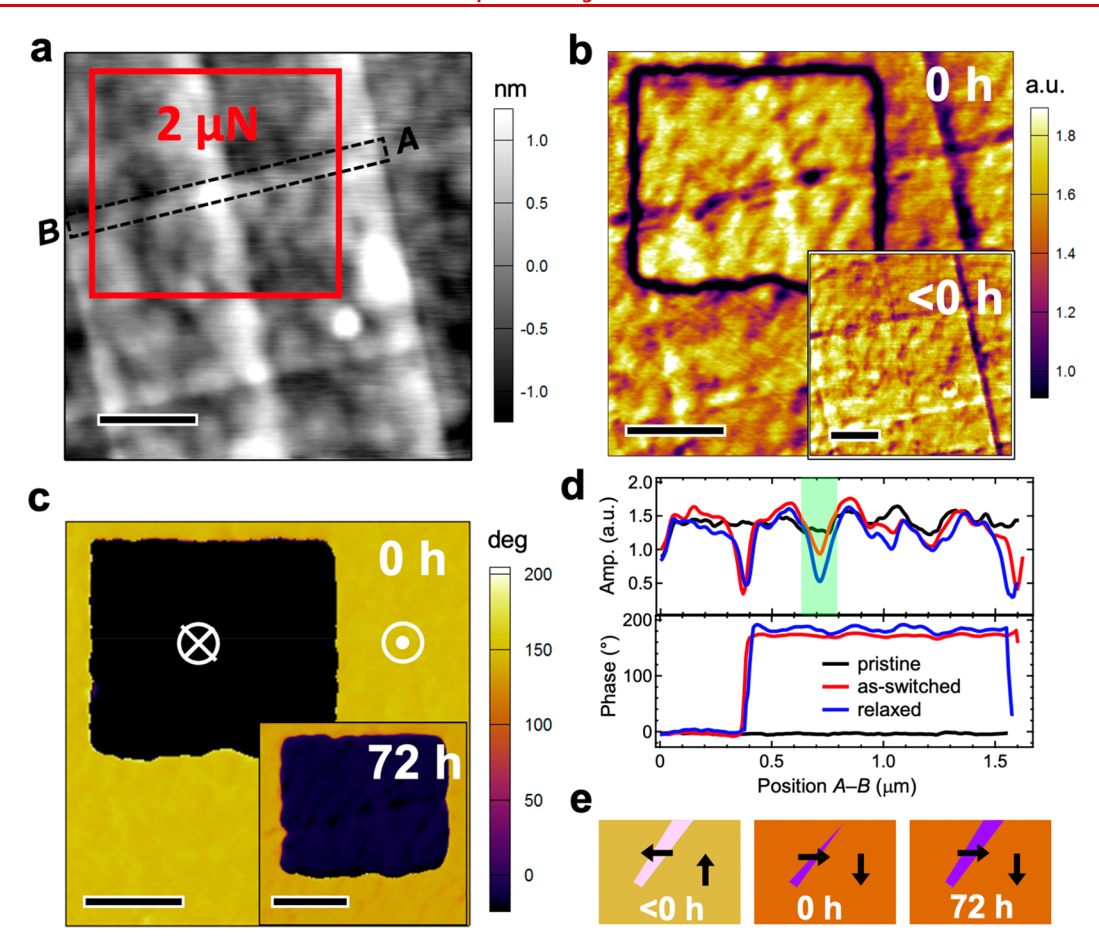


Figure 2. Mechanical switching under strong loading pressure. (a) Surface morphology surrounding a (line-boxed) squared region that was scanned under a loading force of $2 \mu N$ using a Si tip and corresponding (b) PFM amplitude and (c) phase images. Inset to (b) is a PFM amplitude image for the pristine state; inset to (c) is a PFM phase image of the same region measured after 72 h. The symbols in (c) denote the polarization vector directions. For all, scale bar = $0.5 \mu m$. (d) Line profiles of the PFM signals along a ridge averaged over a dash line-boxed region in (a). (e) Schematics for the domain configurations in the three states.

diffraction intensity contrast (Figure 1g, h); similar to the surface morphology, the a'-domains are mainly concentrated at straight-line regions (whose widths are resolution-limited here), while the c-domain matrix shows correlated fluctuations due to certain structural distortions accommodating the a'-domains.

We have further examined the cross-section microstructure of the PZT films down to atomic scales using scanning transmission electron microscopy (STEM). Figure 1i illustrates a typical region containing a single a'-domain with a narrow width of ~ 3 nm, manifested from the derived in-plane strain (ε_{xx}) and lattice spacing maps (Figure 1i-k). This nanodomain extends from the surface at an inclination angle of 45° but terminates inside the film without reaching the SrRuO₃ layer. Similar nanodomains are observed at multiple separated regions in the examined specimen, and some regions contain two parallel a'domains starting from both the surface and PZT/SrRuO₃ interface (see examples in Figure S1a), corroborating the spatial variations revealed in XDM. Compared with conventional fully traversing, thickened ferroelastic domains, 16 these partial a'domains incur additional free energy cost and are typically stabilized by defects such as misfit dislocations⁸ and compositional gradients.²⁸ These extended defects are much less mobile than domain walls under moderate external driving fields and can thus be regarded as local pinning centers against the latter's motion. In addition, electron energy loss spectroscopy mapping confirms no significant Ti/O-element variations across the film

thickness, suggesting good compositional uniformity (Figure S1b).

Next, we explore the mechanical switching behavior of the PZT films within a strong tip-loading force regime. Such a regime is referred to the case when the surface domain of a pressure-scanned region is fully switched and its threshold force is found to vary within $\sim 2-3 \mu N$ for the two types of Si tips used. Figure 2 illustrates the PFM images of a mechanically switched domain in three different states, namely, pristine (<0 h), asswitched (0 h), and relaxed (72 h). Overall, the as-switched domain and surrounding pristine regions exhibit a similar level of PFM amplitude, separated by well-defined domain boundaries where the measured response is markedly reduced (Figure 2b). This, together with a 180° contrast in the corresponding PFM phase images (Figure 2c), confirms an antiparallel polarization arrangement for the adjacent domains after switching. The mechanically switched domains are found to have better stabilities than electrically switched ones, as evaluated by the remnant domain area measured after an elapsed time period. Figure S2a-d presents the evolution of domains switched under 4-8 V tip bias, which all show a lower remnant ratio (<70% after 48 h) as well as worse shape retention than the results in Figure 2c (>90% after 72 h). The reasons for such a difference could be manifold here. First, unlike electric biasing, tip mechanical loading appears not to initiate surface charging and/or electronic charge injection processes (see measured

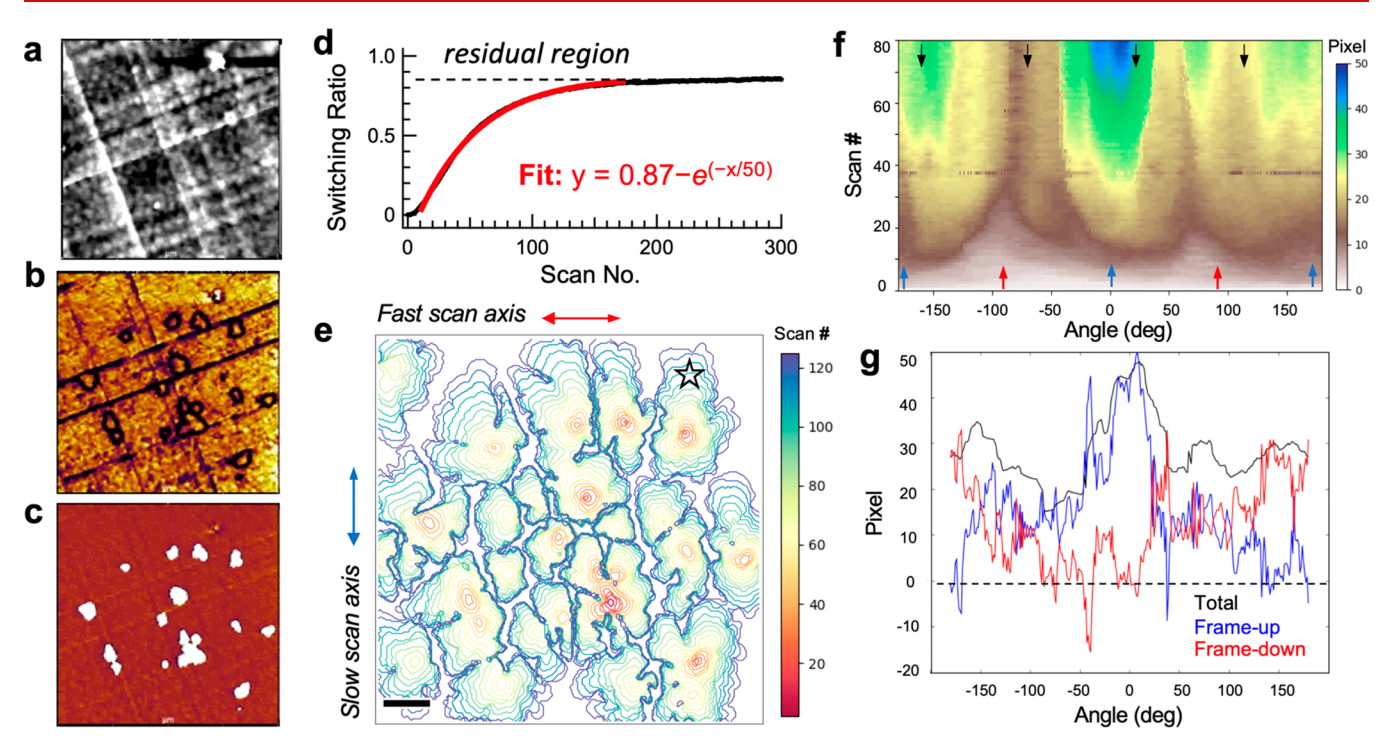


Figure 3. Computer vision analysis of intermediate mechanical switching behavior. A $4 \times 4 \mu m^2$ surface region was continuously scanned under $1.5 \mu N$ using a diamond tip. (a) Surface morphology and (b) piezoresponse amplitude and phase images from the 11th scan. (d) Area ratio of switched domains as a function of scan number along with an exponential fit. (e) Overlay of domain boundary contours from the first 125 PFM images. (f) Angle-resolved evolution of the domain boundary contours emanating from a single nucleation site marked in (e), and (g) is the partial contribution of frame-up/frame-down scans. The red, blue, and black arrows in (f) denote the directions of the fast scan axis, slow scan axis, and the ridge defects of the PZT thin films, respectively.

surface potential contrast in Figure S2e,f) and, hence, may result in better surface screening conditions. Second, the front of mechanically switched domains could penetrate deeper into the films and even reach the bottom electrode, thus forming a more stable arrangement of the polarization vectors. This latter scenario is more presumptive as the effective probing depth (a few tens of nm) in PFM is well below the film thickness. Regardless of the detailed mechanisms, the comparison with electric switching points to the unique characteristics of mechanical switching in the films.

A closer look into the local switching behavior is obtained by tracking the PFM signal profiles along the ridge regions, where the aforementioned a'-domains are known to segregate. The response of these ferroelastic nanodomains to pressure scanning can be distinct from the c-domain matrix, as is indeed corroborated by the line profiles in Figure 2d. Here, we remark on a region (shadowed) with the most appreciable changes. The measured piezoresponse of this region is suppressed after switching and further decays after 72 h. This slow decay process could arise from the relaxation of an a'-domain within the downward switched c-domain matrix; the a'-domain may experience 180° switching and then gradual coarsening, as is tentatively described by the schematics in Figure 2e (also see phase-field simulations below). Similar relaxation phenomena with a time scale of $\sim 10^3$ s were observed in a 60 nm PZT thin film with high-density a-c-domain bundles subject to electric switching.²⁹ Generally, the relaxation of ferroelastic domains can be kinetically controlled by local competing stress and electrostatic environment. In our case, different local environments for the a'-domains could be envisaged as consequences of different polarization coupling manners in the mechanical and

electrical switching cases, which could also be a factor influencing the overall stability of switched c-domains.

While the rearrangement of the a'-domains remains quite subtle from our PFM results, there appears to be a clear correlation between their presence and the mechanical switching behavior of the PZT films. We have first noticed incomplete mechanical switching when the tip gets worn or the tip loading force is not sufficiently high; in both cases the local pressure is in an intermediate regime. Figure S3 presents an example image set of a domain that was gradually switched under 2 μ N using a worn Si tip. These images illustrate that the domain boundary propagates laterally in preferential manners, in addition to the occurrence of new domain nucleation sites. To fully capture such an intermediate switching process, we have modified the PFM measurement scheme. Instead of grounding the tip, we applied a small ac signal (0.5 V_{a.c.}) during pressure scans so as to visualize the domain evolution in real time; besides this, we adopted more durable diamond tips that could withstand several hundreds of consecutive scan frames without obvious degradation. A control experiment performed under a normal imaging force (~250 nN) shows no sign of domain switching over >300 scans (Figure S4), thus ruling out possible effects of the ac probing signal and prolonged scanning itself. By contrast, a striking sequence of domain switching events has been captured in the PFM images measured under ~1500 nN (see

To quantitatively extract the switching information, we have performed a computer vision analysis to the above 1500 nN scan sequence. Figure 3a—c presents an example set of PFM images acquired during the early stage (the 11th scan), where several independent nucleation sites can be observed around the line ridges. These nucleated domains grow sideways during the

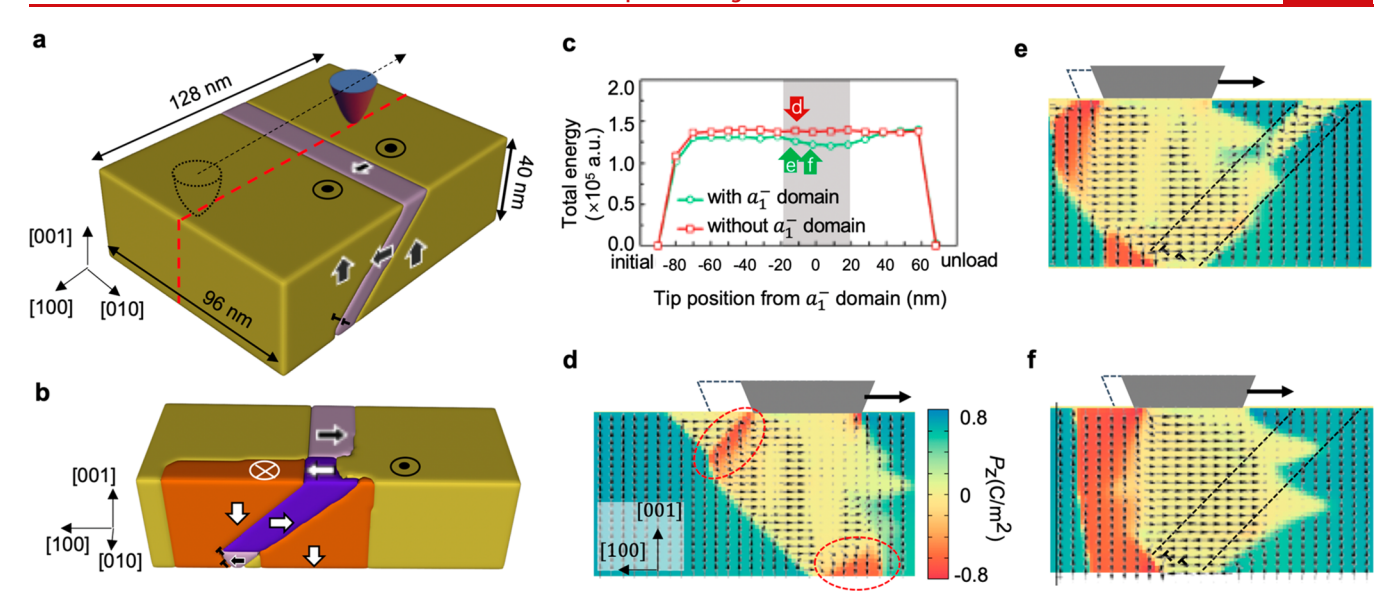


Figure 4. Phase-field simulations of mechanical switching in PZT thin films. (a) Initial domain structure with an a_1^- -domain embedded in a c^+ -domain and pinned by interfacial partial dislocations. The arrows indicate the polarization direction in each domain. The dashed black arrows denote the tip moving path. The dashed red segments denote the cut lines for section views. (b) Final domain structure after the tip scan across the a_1^- -domain. Note only a section cut of the model is presented for clear visualization. (c) Total free energy as a function of tip position during the tip motion. The arrows labeled by d-f correspond to the snapshots in (d-f), respectively. The shaded region denotes the lateral range of the a_1^- -domain along the [100] direction. (d) Snapshot of the polarization distribution under loading for the case without preexisting a_1^- -domain. (e, f) Snapshots of the polarization distribution (e) before and (f) after the penetration of the c^- -domain when the tip approaches the preexisting a_1^- -domain. The color reflects the out-of-plane polarization magnitude P_z . The dashed lines show the contour of the original a_1^- -domain.

subsequent scans and altogether gradually consume the scanned surface region. Nonetheless, under the chosen pressure scan conditions, the mechanically switched domains do not fully consolidate into a single domain matrix; the calculated switching area ratio indicates a total of ~13% residual regions up to ~300 scans. The switching ratio curve follows an exponential law during the nucleation and fast-growth stages (see the fit in Figure 3d), similar to the classical Kolmogorov–Avrami–Ishibashi (KAI) model.^{30,31} The observation of such a trend is novel in itself because it is a locally and mechanically driven polarization switching process, compared with those homogeneous electric-field driven switching processes (typically realized in a capacitor structure) described by the KAI model. During the stagnation stage (after ~200 scans), only sporadic domain motions can be observed at a few regions, suggesting that a larger tip pressure would be required to overcome the energy barrier to initiate domain coalescence. Note that there appears to be no strong correlation between the orientations of the residual domain boundaries and the ridges, suggesting a minor pinning effect by the defects stabilizing the *a*′-domain (Figure S5).

Figure 3e shows an overlay plot of the domain boundary contours for the first 125 scans, providing a direct visualization of the anisotropic domain growth process emanating from multiple nucleation sites. Overall, this growth anisotropy appears to be correlated with the topographic defect ridges (Figure 3a). At some regions, the domain boundary fronts were accelerated along the ridges and remarkably decelerated perpendicular to them (so the contour distribution is squeezed wherein), yet at other regions, the domain fronts could readily propagate across the ridges. Such qualitative differences among the ridges must be associated with their specific a'-domain configurations coupled with the tip scan manners. The former factor is known to vary spatially to certain extent in the films from the structural characterizations, and here, its influence on mechanical switching can be delineated from local analyses of

the specific domain growth kinetics. Figure 3f presents an example of the angle-resolved domain growth analyses (see examples for another two nucleation sites in Figure S5), which clearly reveals fast/slow domain growth rates for the two orthogonal directions with respect to the main defect ridges, in addition to minor fluctuations which might be attributed to the presence of other defect types. Moreover, the contributions from the frame-up/down scans can be decomposed to highlight the influence of the tip scan manners, as illustrated in Figure 3g. Note that here each of the image frames are comprised of twoway interweaved fast-scan directions, and in principle, their contributions can be further decomposed. A marked difference can be found around the $0^{\circ}/180^{\circ}$ orientations, indicating that the domain outward growth parallel to the slow scan axes is favored. The scan axes determine both the real-time traction distribution of tip pressure and its alignment with the preexisting domain fronts. Thus, these results suggest ways to controlling the domain growth kinetics via controlled tip motion, consistent with a few previous studies. 21,32

To understand the observed mechanical switching behavior, we have performed phase-field simulations incorporating a maximum degree of realistic experimental conditions (see the model setup details in the Methods within the Supporting Information). 33-35 Note that the influence of flexoelectricity on the switching process is found to be marginal, due to high intrinsic switching barriers of PZT and large film thickness (relative to ultrathin BaTiO₃^{9,23,25}), and hence is not considered for the results presented here. As illustrated in Figure 4a, the model system is a 40 nm PZT20/80 thin film assuming an upward-polarized initial state with an embedded a_1^+ -domain (with polarization along the [100]) pinned by a pair of partial dislocations at the interface. 8,36 Under a biaxial substrate misfit strain of -1.0%, the size of the a_1^+ -domain is comparable to the experimentally observed a'-domains. The tip scans across the a_1^+ domain with a moving rate of 10 nm/10000 timesteps with a

corresponding frictional traction proportional to the normal load. The final domain state at equilibrium after the tip scanning across the a_1^+ -domain and being released is shown in Figure 4b (also see the entire domain evolution in Movie S2). The occurrence of 180° polarization switching is observed for both the initial c^+ -domain and the embedded a_1^+ -domain along the tip scanning path. Significantly, this behavior is not reproduced under similar conditions for the model without a preexisting a_1^+ -domain (see Movie S3) nor the model with a preexisting but unpinned a_1^+ -domain (see Figure S6). In the former case, even though 90° and 180° domain switching occurs locally following the tip contact region, there is no complete domain switching after unloading; instead, the system reverts to the single c^+ -domain state.

To reveal the critical role of the preexisting a_1^+ -domain on enabling the 180° switching, we examine the total free energy changes of the system as a function of tip position in Figure 4c. A dip in the free energy is seen when the tip scans across the a_1^+ domain, suggesting a lower-energy transition pathway associated with the formation of different domain configurations due to the preexisting ferroelastic nanodomain. Such differences are illustrated by snapshots of the equilibrium polarization distribution for three timesteps in Figure 4d-f. When the a_1^+ domain is absent (Figure 4d), mechanical loading can induce 90° switching (from the c^+ to a majority of a_1^- and a small portion of a_2^{\pm}) throughout the film thickness. Meanwhile, it can also nucleate 180° domains (from the c^{+} to c^{-}) near the surface both behind the contact region and at the interface in front of the tip (see two circled regions in Figure 4d), due to a synergic effect of compressive and shear stress imposed by the moving tip.^{24,37} However, the two localized c^- -domain nuclei move concomitantly with the tip motion, precluding their connection and penetration through the film thickness, that is, an uncompleted 180° switching. When there exists an embedded a_1^+ -domain, the c^- domain nucleus at the bottom is pinned at the junction between the a_1^+ -domain and the interface (Figure 4e), which allows for its merging with the nucleus at the surface when the tip scans across the junction (Figure 4f), thus completing the 180° switching. Such a complete c^- -domain remains stable after unloading and facilitates the 180° switching of its adjacent c^+ domain regions during subsequent pressure scans. Additionally, the tip-induced a_1^- -domain intersects with the preexisting a_1^+ domain, giving rise to a complex interaction among the four nanosized a-domains (see Movie S2). This interaction may account for the relaxation behavior aforementioned in Figure 2d,e. Thus, our simulations demonstrate the feasibility to mechanically realize 180° polarization switching through unusual domain nucleation and growth processes mediated by the presence of a'-domains, constituting an alternative mechanism for material systems where the recognized flexoelectricity-based mechanism could not dominate.

DISCUSSION AND CONCLUSION

In summary, we have observed robust mechanical switching in tetragonal-phase PZT films with a large thickness of ~ 100 nm. This switching behavior is intimately correlated with the microstructure of the films which consists of nanosized a'-domains embedded in a c-domain matrix, with the a'-domains playing a critical role in the switching nucleation process. Phasefield simulations further reveal the mechanisms of ferroelastic nanodomains in dynamically mediating 180° polarization switching in thick PZT films. Altogether, our study suggests new strategies to design ferroelectric materials with tailored

microstructures for mechanical switching as opposed to pursuing highly uniform, ultrathin films. Apart from epitaxial strain engineering, of particular note is novel compositional gradient thin-film epitaxy, as has been demonstrated to introduce highly mobile needle-like ferroelastic domains in PZT films. 28 These complex microstructures may host diverse electromechanical coupling mechanisms that enable mechanical switching beyond the narrow scope of flexoelectricity, thus expanding its application potentials in (multi)ferroic devices. Moreover, our findings may have far-reaching implications for understanding electromechanical performance of many ferroelectric material families such as BiFeO₃ and Hf_{0.5}Zr_{0.5}O₂.³⁸ In these materials, dynamical coupling of external driving fields with flattened free-energy landscapes, often associated with their hierarchical ferroelastic microstructure, may lead to competing local domain switching pathways and ultimately regulate their functional response.

ASSOCIATED CONTENT

Supporting Information

The Supporting Information is available free of charge at https://pubs.acs.org/doi/10.1021/acs.nanolett.0c03875.

Methods, including sample growth, synchrotron XRD, STEM, PFM, and phase-field simulation analyses, and Figures S1–S6 (PDF)

Movie S1 (MOV)

Movie S2 (MOV)

Movie S3 (MOV)

AUTHOR INFORMATION

Corresponding Authors

Qian Li — State Key Laboratory of New Ceramics and Fine Processing, School of Materials Science and Engineering, Tsinghua University, Beijing 100084, China; Center for Nanophase Materials Science, Oak Ridge National Laboratory, Oak Ridge, Tennessee 37831, United States; orcid.org/0000-0001-7922-598X; Email: qianli_mse@tsinghua.edu.cn

Sergei V. Kalinin — Center for Nanophase Materials Science, Oak Ridge National Laboratory, Oak Ridge, Tennessee 37831, United States; orcid.org/0000-0001-5354-6152; Email: sergei2@ornl.gov

Jing-Feng Li — State Key Laboratory of New Ceramics and Fine Processing, School of Materials Science and Engineering, Tsinghua University, Beijing 100084, China; orcid.org/0000-0002-0185-0512; Email: jingfeng@mail.tsinghua.edu.cn

Authors

Bo Wang — Department of Materials Science and Engineering, Pennsylvania State University, University Park, Pennsylvania 16802, United States

Qian He — Department of Materials Science and Engineering, National University of Singapore, Singapore 119077; orcid.org/0000-0003-4891-3581

Pu Yu – State Key Laboratory of Low Dimensional Quantum Physics and Department of Physics, Tsinghua University, Beijing 100084, China

Long-Qing Chen — Department of Materials Science and Engineering, Pennsylvania State University, University Park, Pennsylvania 16802, United States

Complete contact information is available at:

https://pubs.acs.org/10.1021/acs.nanolett.0c03875

Author Contributions

[#]QL and BW contributed equally to this study.

Author Contributions

Q.L., S.V.K., and J.F.L. designed the study. Q.L. conducted PFM and XRD measurements. B.W. and L.Q.C. performed phase-field simulations. Q.H. performed STEM measurements. P.Y. fabricated the materials. Q.L. wrote the manuscript with input from all the authors.

Notes

The authors declare no competing financial interest.

ACKNOWLEDGMENTS

This work was supported by the Basic Science Center Project of NSFC under grant no. 51788104 and the National Key Basic Research Program of China under grant no. 2020YFA0309100. B.W. and L.-Q.C. acknowledge the support by National Science Foundation (NSF) through grant no. DMR-1744213. A portion of this research was conducted at the Center for Nanophase Materials Sciences, which is a U.S. Department of Energy (DOE) Office of Science User Facility. This research used resources of the Advanced Photon Source, a U.S. DOE Office of Science User Facility operated for the DOE Office of Science by Argonne National Laboratory under contract no. DE-AC02-06CH11357.

REFERENCES

- (1) Kalinin, S. V.; Morozovska, A. N.; Chen, L. Q.; Rodriguez, B. J. Local Polarization Dynamics in Ferroelectric Materials. *Rep. Prog. Phys.* **2010**, *73* (5), 056502.
- (2) Kim, D. J.; Lu, H.; Ryu, S.; Bark, C.-W.; Eom, C.-B.; Tsymbal, E. Y.; Gruverman, A. Ferroelectric Tunnel Memristor. *Nano Lett.* **2012**, *12* (11), 5697–5702.
- (3) Wang, Z.; Wu, H.; Burr, G. W.; Hwang, C. S.; Wang, K. L.; Xia, Q.; Yang, J. J. Resistive Switching Materials for Information Processing. *Nature Reviews Materials* **2020**, *5* (3), 173–195.
- (4) Yang, S.; Peng, R.-C.; He, Q.; Huang, Y.-L.; Huang, Y.; Yang, J.-C.; Chen, T.; Guo, J.; Chen, L.-Q.; Chu, Y.-H.; Nan, C.-W.; Yu, P. Electric Field Writing of Ferroelectric Nano-Domains Near 71° Domain Walls with Switchable Interfacial Conductivity. *Ann. Phys.* **2018**, 530 (8), 1800120
- (5) Wen, Z.; Li, C.; Wu, D.; Li, A.; Ming, N. Ferroelectric-Field-Effect-Enhanced Electroresistance in Metal/Ferroelectric/Semiconductor Tunnel Junctions. *Nat. Mater.* **2013**, *12* (7), 617–621.
- (6) Ma, J.; Ma, J.; Zhang, Q.; Peng, R.; Wang, J.; Liu, C.; Wang, M.; Li, N.; Chen, M.; Cheng, X.; Gao, P.; Gu, L.; Chen, L.-Q.; Yu, P.; Zhang, J.; Nan, C.-W. Controllable Conductive Readout in Self-Assembled, Topologically Confined Ferroelectric Domain Walls. *Nat. Nanotechnol.* **2018**, *13* (10), 947–952.
- (7) Heo, Y.; Sharma, P.; Liu, Y. Y.; Li, J. Y.; Seidel, J. Mechanical Probing of Ferroelectrics at the Nanoscale. *J. Mater. Chem. C* **2019**, 7 (40), 12441–12462.
- (8) Gao, P.; Britson, J.; Nelson, C. T.; Jokisaari, J. R.; Duan, C.; Trassin, M.; Baek, S.-H.; Guo, H.; Li, L.; Wang, Y.; Chu, Y.-H.; Minor, A. M.; Eom, C.-B.; Ramesh, R.; Chen, L.-Q.; Pan, X. Ferroelastic Domain Switching Dynamics under Electrical and Mechanical Excitations. *Nat. Commun.* **2014**, *5*, 3801.
- (9) Lu, H.; Bark, C. W.; Esque de los Ojos, D.; Alcala, J.; Eom, C. B.; Catalan, G.; Gruverman, A. Mechanical Writing of Ferroelectric Polarization. *Science* **2012**, 336 (6077), 59–61.
- (10) Lu, H.; Wang, B.; Li, T.; Lipatov, A.; Lee, H.; Rajapitamahuni, A.; Xu, R.; Hong, X.; Farokhipoor, S.; Martin, L. W.; Eom, C.-B.; Chen, L.-Q.; Sinitskii, A.; Gruverman, A. Nanodomain Engineering in Ferroelectric Capacitors with Graphene Electrodes. *Nano Lett.* **2016**, *16* (10), 6460–6466.

- (11) Lu, H.; Lee, D.; Klyukin, K.; Tao, L.; Wang, B.; Lee, H.; Lee, J.; Paudel, T. R.; Chen, L.-Q.; Tsymbal, E. Y.; Alexandrov, V.; Eom, C.-B.; Gruverman, A. Tunneling Hot Spots in Ferroelectric SrTiO₃. *Nano Lett.* **2018**, *18* (1), 491–497.
- (12) Lee, D.; Lu, H.; Gu, Y.; Choi, S.-Y.; Li, S.-D.; Ryu, S.; Paudel, T. R.; Song, K.; Mikheev, E.; Lee, S.; Stemmer, S.; Tenne, D. A.; Oh, S. H.; Tsymbal, E. Y.; Wu, X.; Chen, L.-Q.; Gruverman, A.; Eom, C. B. Emergence of Room-Temperature Ferroelectricity at Reduced Dimensions. *Science* **2015**, 349 (6254), 1314–1317.
- (13) Sharma, P.; Ryu, S.; Viskadourakis, Z.; Paudel, T. R.; Lee, H.; Panagopoulos, C.; Tsymbal, E. Y.; Eom, C.-B.; Gruverman, A. Electromechanics of Ferroelectric-Like Behavior of LaAlO3 Thin Films. *Adv. Funct. Mater.* **2015**, *25* (41), 6538–6544.
- (14) Zubko, P.; Catalan, G.; Tagantsev, A. K. Flexoelectric Effect in Solids. *Annu. Rev. Mater. Res.* **2013**, *43* (1), 387–421.
- (15) Wang, B.; Gu, Y.; Zhang, S.; Chen, L.-Q. Flexoelectricity in Solids: Progress, Challenges, and Perspectives. *Prog. Mater. Sci.* **2019**, *106*, 100570.
- (16) Lu, X.; Chen, Z.; Cao, Y.; Tang, Y.; Xu, R.; Saremi, S.; Zhang, Z.; You, L.; Dong, Y.; Das, S.; Zhang, H.; Zheng, L.; Wu, H.; Lv, W.; Xie, G.; Liu, X.; Li, J.; Chen, L.; Chen, L.-Q.; Cao, W.; Martin, L. W. Mechanical-Force-Induced Non-Local Collective Ferroelastic Switching in Epitaxial Lead-Titanate Thin Films. *Nat. Commun.* **2019**, *10* (1), 1–8.
- (17) Li, Q.; Cao, Y.; Yu, P.; Vasudevan, R.; Laanait, N.; Tselev, A.; Xue, F.; Chen, L.; Maksymovych, P.; Kalinin, S.; Balke, N. Giant Elastic Tunability in Strained BiFeO3 near an Electrically Induced Phase Transition. *Nat. Commun.* **2015**, *6*, 8985.
- (18) Cao, Y.; Yang, S.; Jesse, S.; Kravchenko, I.; Yu, P.; Chen, L.-Q.; Kalinin, S. V.; Balke, N.; Li, Q. Exploring Polarization Rotation Instabilities in Super-Tetragonal BiFeO₃ Epitaxial Thin Films and Their Technological Implications. *Advanced Electronic Materials* **2016**, 2 (12), 1600307.
- (19) Hong, S.; Tong, S.; Park, W. I.; Hiranaga, Y.; Cho, Y.; Roelofs, A. Charge Gradient Microscopy. *Proc. Natl. Acad. Sci. U. S. A.* **2014**, *111* (18), 6566–6569.
- (20) Das, S.; Wang, B.; Cao, Y.; Rae Cho, M.; Jae Shin, Y.; Mo Yang, S.; Wang, L.; Kim, M.; Kalinin, S. V.; Chen, L.-Q.; Noh, T. W. Controlled Manipulation of Oxygen Vacancies Using Nanoscale Flexoelectricity. *Nat. Commun.* **2017**, *8* (1), 615.
- (21) Park, S. M.; Wang, B.; Das, S.; Chae, S. C.; Chung, J.-S.; Yoon, J.-G.; Chen, L.-Q.; Yang, S. M.; Noh, T. W. Selective Control of Multiple Ferroelectric Switching Pathways Using a Trailing Flexoelectric Field. *Nat. Nanotechnol.* **2018**, *13* (5), 366–370.
- (22) Cao, Y.; Morozovska, A.; Kalinin, S. V. Pressure-Induced Switching in Ferroelectrics: Phase-Field Modeling, Electrochemistry, Flexoelectric Effect, and Bulk Vacancy Dynamics. *Phys. Rev. B: Condens. Matter Mater. Phys.* **2017**, *96* (18), 184109.
- (23) Chen, W.; Liu, J.; Ma, L.; Liu, L.; Jiang, G. L.; Zheng, Y. Mechanical Switching of Ferroelectric Domains beyond Flexoelectricity. *J. Mech. Phys. Solids* **2018**, *111*, 43–66.
- (24) Ma, L. L.; Chen, W. J.; Liu, Y. L.; Wang, B.; Zheng, Y. On the Mechanisms of Tip-Force Induced Switching in Ferroelectric Thin Films: The Crossover of Depolarization, Shear Strain and Flexoelectricity. *J. Phys.: Condens. Matter* **2019**, *31* (14), 145701.
- (25) Wang, B.; Lu, H.; Bark, C. W.; Eom, C.-B.; Gruverman, A.; Chen, L.-Q. Mechanically Induced Ferroelectric Switching in BaTiO₃ Thin Films. *Acta Mater.* **2020**, *193*, 151–162.
- (26) Sheng, G.; Hu, J. M.; Zhang, J. X.; Li, Y. L.; Liu, Z. K.; Chen, L. Q. Phase-Field Simulations of Thickness-Dependent Domain Stability in PbTiO₃ Thin Films. *Acta Mater.* **2012**, *60* (8), 3296–3301.
- (27) Li, Q.; Marks, S. D.; Bean, S.; Fisher, M.; Walko, D. A.; DiChiara, A. D.; Chen, X.; Imura, K.; Sato, N. K.; Liu, M.; Evans, P. G.; Wen, H. Simultaneous Scanning Near-Field Optical and X-Ray Diffraction Microscopy for Correlative Nanoscale Structure—Property Characterization. J. Synchrotron Radiat. 2019, 26 (5), 1790–1796.
- (28) Agar, J. C.; Damodaran, A. R.; Okatan, M. B.; Kacher, J.; Gammer, C.; Vasudevan, R. K.; Pandya, S.; Dedon, L. R.; Mangalam, R. V. K.; Velarde, G. A.; Jesse, S.; Balke, N.; Minor, A. M.; Kalinin, S. V.;

- Martin, L. W. Highly Mobile Ferroelastic Domain Walls in Compositionally Graded Ferroelectric Thin Films. *Nat. Mater.* **2016**, *15*, 549.
- (29) Ivry, Y.; Wang, N.; Chu, D.; Durkan, C. 90 Domain Dynamics and Relaxation in Thin Ferroelectric/Ferroelastic Films. *Phys. Rev. B: Condens. Matter Mater. Phys.* **2010**, *81* (17), 174118.
- (30) Tagantsev, A. K.; Stolichnov, I.; Setter, N.; Cross, J. S.; Tsukada, M. Non-Kolmogorov-Avrami Switching Kinetics in Ferroelectric Thin Films. *Phys. Rev. B: Condens. Matter Mater. Phys.* **2002**, *66* (21), 214109.
- (31) Hu, W. J.; Juo, D.-M.; You, L.; Wang, J.; Chen, Y.-C.; Chu, Y.-H.; Wu, T. Universal Ferroelectric Switching Dynamics of Vinylidene Fluoride-Trifluoroethylene Copolymer Films. *Sci. Rep.* **2015**, *4* (1), 4772.
- (32) Wang, C.; Ke, X.; Wang, J.; Liang, R.; Luo, Z.; Tian, Y.; Yi, D.; Zhang, Q.; Wang, J.; Han, X.-F.; Van Tendeloo, G.; Chen, L.-Q.; Nan, C.-W.; Ramesh, R.; Zhang, J. Ferroelastic Switching in a Layered-Perovskite Thin Film. *Nat. Commun.* **2016**, *7* (1), 10636.
- (33) Chen, L.-Q. Phase-Field Method of Phase Transitions/Domain Structures in Ferroelectric Thin Films: A Review. *J. Am. Ceram. Soc.* **2008**, *91* (6), 1835–1844.
- (34) Wang, J.-J.; Wang, B.; Chen, L.-Q. Understanding, Predicting, and Designing Ferroelectric Domain Structures and Switching Guided by the Phase-Field Method. *Annu. Rev. Mater. Res.* **2019**, 49 (1), 127–152.
- (35) Haun, M. J.; Furman, E.; Jang, S. J.; Cross, L. E. Thermodynamic Theory of the Lead Zirconate-Titanate Solid Solution System, Part V: Theoretical Calculations. *Ferroelectrics* **1989**, *99* (1), 63–86.
- (36) Britson, J.; Nelson, C.; Pan, X.; Chen, L.-Q. First-Order Morphological Transition of Ferroelastic Domains in Ferroelectric Thin Films. *Acta Mater.* **2014**, *75*, 188–197.
- (37) Chen, W. J.; Yuan, S.; Ma, L. L.; Ji, Y.; Wang, B.; Zheng, Y. Mechanical Switching in Ferroelectrics by Shear Stress and Its Implications on Charged Domain Wall Generation and Vortex Memory Devices. *RSC Adv.* **2018**, *8* (8), 4434–4444.
- (38) Wei, Y.; Nukala, P.; Salverda, M.; Matzen, S.; Zhao, H. J.; Momand, J.; Everhardt, A. S.; Agnus, G.; Blake, G. R.; Lecoeur, P.; Kooi, B. J.; Íñiguez, J.; Dkhil, B.; Noheda, B. A Rhombohedral Ferroelectric Phase in Epitaxially Strained Hf_{0.5}Zr_{0.5}O₂ Thin Films. *Nat. Mater.* **2018**, *17* (12), 1095–1100.